

## SOFT X-RAY EXCESS EMISSION IN CLUSTERS OF GALAXIES OBSERVED WITH XMM-NEWTON

J. NEVALAINEN<sup>1,2,3</sup>, R. LIEU<sup>2</sup>, M. BONAMENTE<sup>2</sup>, D. LUMB<sup>3</sup>Harvard - Smithsonian Center for Astrophysics, Cambridge, USA<sup>1</sup>University of Alabama in Huntsville, Huntsville, USA<sup>2</sup>ESTEC, Noordwijk, Netherlands<sup>3</sup>*ApJ*, accepted Oct 28, 2002

## ABSTRACT

We present results on the spectroscopic analysis of XMM-Newton EPIC data of the central  $0.5 h_{50}^{-1}$  Mpc regions of the clusters of galaxies Coma, A1795 and A3112. The temperature of the hot intracluster gas as determined by modeling the 2 – 7 keV PN and MOS data is consistent with that inferred from the FeXXV-FeXXVI line ratio. A significant warm emission component at a level above the systematic uncertainties is evident in the data and confirmed by ROSAT PSPC data for Coma and A1795. The non-thermal origin of the phenomenon cannot be ruled out at the current level of calibration accuracy, but the thermal model fits the data significantly better, with temperatures in the range of 0.6 – 1.3 keV and electron densities of the order of  $10^{-4} - 10^{-3} \text{ cm}^{-3}$ . In the outer parts of the clusters the properties of the warm component are marginally consistent with the results of recent cosmological simulations, which predict a large fraction of the current epoch's bayons located in a warm-hot intergalactic medium (WHIM). However, the derived densities are too high in the cluster cores, compared to WHIM simulations, and thus more theoretical work is needed to fully understand the origin of the observed soft X-ray excess.

*Subject headings:* galaxies: clusters – X-rays: galaxies

## 1. INTRODUCTION

In 1996, Lieu et al. (1996a,b) reported the discovery of excess EUV and soft X-ray emission above the contribution from the hot ICM in the nearby Virgo and Coma clusters using data from Extreme UltraViolet Explorer (*EUVE*) and ROSAT PSPC. Later, EUV excess emission was detected by *EUVE* in A1795 by Mittaz, Lieu and Lockman (1998) and in A2199 by Lieu, Bonamente and Mittaz (1999a); these results were disputed by Bowyer, Berghoefer and Korpela (1999), and further affirmed by Lieu et al. (1999b; A2199) Bonamente, Lieu and Mittaz (2001a; A1795 and Virgo). The *BeppoSAX* LECS instrument provided also a positive detection of excess emission in A3571 (Bonamente et al. 2001c) and A2199 (Kaastra et al. 1999), the latter challenged by Berghoefer and Bowyer (2002) yet rebutted by Kaastra et al. (2002). Analysis of ROSAT PSPC data has yielded further evidence for soft X-ray excess emission in Coma (Arabadjis and Bregman, 1999), Virgo (Buote, 2001; Bonamente Lieu and Mittaz, 2001b), Shapley (Bonamente et al. 2001c) and Sérsic 159-03 (Bonamente, Lieu and Mittaz 2001d). Recently, a sample of clusters studied with PSPC yielded significant soft excess emission in  $\sim 50\%$  of the clusters (Bonamente et al. 2002).

Possible scenarios, involving thermal or non-thermal emission, for the origin of the soft excess have been proposed since the discovery of the phenomenon. The thermal model requires large amounts of warm baryons (Lieu et al 1996a,b; Mittaz, Lieu & Lockman 1998; see also Bonamente et al 2001b,c,d). They are currently believed to reside in warm-hot *inter*-cluster filaments, as recently modeled in large-scale hydrodynamical simulations (e.g., Cen et al. 1999,2001; Dave et al. 2001). In the non-thermal model the soft excess is due to inverse-Compton interaction between the cosmic microwave background and a pop-

ulation of intracluster relativistic electrons (Hwang 1997, Sarazin & Lieu 1998, Lieu et al. 1999).

The previously analyzed ROSAT PSPC data indicate that the excess emission is probably of thermal origin, although the limited spectral resolution of PSPC could not completely rule out the presence of non-thermal radiation (e.g., Bonamente et al. 2002). The superior spectral resolution, the large bandpass coverage (0.2 – 10 keV) and the large collecting area of the XMM-Newton EPIC makes it well suited for studying the soft excess phenomenon. With EPIC, one can for the first time constrain simultaneously the properties of the hot gas and the soft component in clusters of galaxies. In this work we analyse the PN and MOS data from the central  $0.5 h_{50}^{-1}$  Mpc regions of clusters Coma, A1795 and A3112. We will present results on the detection and modeling of the soft component and outline a possible scenario responsible for this phenomenon. We will study the accuracy of the EPIC calibration by comparing our results with those of the reported EPIC calibration activities, and with the published ROSAT PSPC data.

We consider uncertainties and significances at 90% confidence level, and use  $H = 50 \times h_{50} \text{ km s}^{-1} \text{ Mpc}^{-1}$ , unless stated otherwise.

## 2. DATA ANALYSIS

The data used in this work are taken from XMM-Newton public data archive (Coma and A1795) and from the Guaranteed Time program (A3112). We used the pipeline processed products of Coma and A1795 and processed the A3112 data using *epchain* and *emchain* tools in SAS 5.2.0. Among the clusters available to us at the time of this writing, only these three were bright enough for our analysis. For the details of the observations of Coma and A1795 we refer to the previous published analyses of some of these data (Coma: Arnaud et al. 2001a; A1795:

TABLE 1

Basic information on the observations

cluster	z	obs id	obs date yyyy-mm-dd	livetime <sup>a</sup> ks			count rate cut <sup>b</sup>			exposure <sup>c</sup> ks			filter
				PN	M1	M2	PN	M1	M2	PN	M1	M2	
Coma	0.023	0153750101	2001-12-04	20	25	25	55	15	15	17	21	20	medium
A1795	0.062	009782010	2000-06-26	42	48	48	50	15	25	23	29	32	thin
A3112	0.076	0105660101	2000-12-24	17	23	23	50	15	15	17	22	22	medium

a: central CCD, after pipeline processing

b: counts in 100s bin at 12 – 14 keV (PN) and 10 – 12 keV (MOS)

c: after filtering the flares

Arnaud et al. 2001b, Tamura et al. 2001). We report the basic information of the specific data used in our work in Table 1. All the data are obtained in the full frame mode of the EPIC cameras.

In order to identify the periods of significant soft proton flares, we extracted light curves of the cluster data in 100s bins and for energies  $\geq 10$  keV, where the cluster contribution is negligible due to the low effective area (see e.g. Marty et al. 2002). If the count rate in a given time bin exceeds our limits (see Table 1), we will exclude that bin at the spectrum extraction stage. The light curves show that A3112 data are free of strong flares but have some short term spikes. There is a strong flare towards the end of the observation of Coma, excluding which reduces the useful exposure time by 20%. There are several strong flares during the observation of A1795, reducing the useful exposure by 50%. After the flare filtering, there remains enough photons for our analysis in all clusters.

We extracted the cluster spectra using only photons designated with patterns 0 for PN and 0 – 12 for MOS. Excising point sources and bad pixels, we obtained the spectra in two large radial bins, 0-0.2-0.5  $h_{50}^{-1}$  Mpc, which correspond to 0-5.2'-13.0' for Coma, 0-2.1'-5.1' for A1795 and 0-1.7'-4.3' for A3112. For the energy redistribution of PN, MOS1 and MOS2 we use the calibration files `epn_ff20_sY9.rmf`, `m1_r5_all_15.rmf` and `m2_r5_all_15.rmf`, respectively. We created the effective area files with `arfgen-1.44.4` tool within SAS distribution, using the calibration information available in March 2002.

For the background estimate, we used the blank sky data (Lumb et al. 2002) extracted at the same detector coordinates as the source spectra, using the same count rate criteria in the  $> 10$  keV band as for the data. We limit our spectral analysis to 0.3 – 7.0 keV band to ensure that at low energies the source signal level is more than 10 times above that of the background and 5 times at the highest energies. This is needed to avoid any errors in the background subtraction, as explained below. We use the 12 – 14 keV (PN) and 10 – 12 keV (MOS) band of source and background data to normalize the background to correspond the background level during the cluster observations. Here we effectively assume that any excess background has the same spectral shape as the blank sky.

While the spectra due to the possible residual soft proton flares may be different from the blank sky spectrum, the above assumption has no effect on our results: Owing to the adopted criteria for the ratio of source to background levels, the typical background variation by 10 – 20 % leads to smaller than 5% variations in the background subtracted data, i.e. below the level of systematic uncertainties. The blank sky data were obtained with a thin filter, while Coma and A3112 observations were made with the medium filter. Although the effective area of PN for the thin filter is 50% higher than that for the medium filter at 0.3 keV, the difference reduces to 1% at 1 keV, then the small background at low energies results in a maximum over-subtraction of less than 5% at all energies.

We binned the spectra to achieve at least 20 counts per bin, and further required that the energy resolution (FWHM) is oversampled by less than a factor of 3. We determined this resolution at different energies by using XSPEC to fold a narrow Gaussian at a given energy and measuring the energies where the redistributed counts drop below 0.5 of the peak value. At  $< 0.5$  keV this is not feasible due to strong deviation of the energy redistribution function from the gaussian shape, i.e. even if the FWHM was small, the broad shoulders distribute the counts much further. We thus used the FWHM values found at 0.5 keV for lower energies. The resulting FWHM values range from 90 eV to 160 eV between energies 0.5 keV and 7 keV.

### 3. IRON LINE RATIO AS THERMOMETER

Because of the possible problems with the calibration of the spectral response of PN and MOS, we first seek a way of characterizing the hot component without relying on the continuum. Such a tool is the temperature-dependent flux ratio of the emission lines due to FeK $\alpha$  transition: iron XXV (helium-like) and XXVI (hydrogen-like). These lines cover a very narrow band ( $\sim 300$  eV) at 6 - 7 keV at these redshifts and thus are quite insensitive to the details of the effective area function. The energy resolution of PN ( $\sim 150$  eV FWHM) at 6 keV is adequate to resolve these lines separately. Also, the number of the line emission photons in Coma and A1795 ( $\sim 1000$ ) renders the ratio measurable in these clusters.

TABLE 2

Comparison of different temperature measurements. “Mekal” refers to fitting 2 - 7 keV band with absorbed mekal model (repeated from Table 4), “cont” corresponds to fitting the 2 - 6 keV energy band with absorbed bremsstrahlung model, and “Fe” to the FeXXV – FeXXVI line ratio measurement

radii	PN			MOS	PN+MOS
	$T_{Fe}$ (keV)	$T_{cont}$ (keV)	$T_{mekal}$ (keV)	$T_{mekal}$ (keV)	$T_{mekal}$ (keV)
<b>Coma</b>					
0'– 5'	$8.7^{+2.1}_{-1.4}$	$9.2^{+0.9}_{-0.6}$	$9.2^{+0.7}_{-0.6}$	$9.9^{+0.6}_{-0.5}$	$9.6^{+0.4}_{-0.3}$
5'– 13'	$7.7^{+1.0}_{-1.0}$	$9.5^{+0.8}_{-0.6}$	$9.2^{+0.6}_{-0.5}$	$9.8^{+0.6}_{-0.4}$	$9.6^{+0.3}_{-0.3}$
<b>A1795</b>					
0'– 2'	$5.4^{+0.6}_{-0.6}$	$5.2^{+0.3}_{-0.2}$	$5.4^{+0.2}_{-0.3}$	$5.5^{+0.3}_{-0.2}$	$5.5^{+0.1}_{-0.1}$
2'– 5'	$6.0^{+0.7}_{-1.0}$	$6.6^{+0.5}_{-0.5}$	$6.7^{+0.4}_{-0.4}$	$6.9^{+0.4}_{-0.3}$	$6.8^{+0.1}_{-0.2}$
<b>A3112</b>					
0'– 1.5'	...	$4.3^{+0.3}_{-0.2}$	$4.6^{+0.3}_{-0.2}$	$4.9^{+0.3}_{-0.2}$	$4.8^{+0.2}_{-0.1}$
1.5'– 4.5'	...	$5.2^{+0.6}_{-0.5}$	$5.4^{+0.5}_{-0.4}$	$5.1^{+0.4}_{-0.4}$	$5.2^{+0.3}_{-0.2}$

### 3.1. Model

To obtain a model for the line flux ratio as a function of temperature, we used the XSPEC model MEKAL and PN responses to simulate spectra for a grid of temperatures with a step size of 0.1 keV, keeping metal abundance at 0.3 of solar value, and normalization fixed to unity in XSPEC units. Since the fluxes of the FeXXV and FeXXVI lines have the same dependence on the metal abundance, as well as on the overall model normalization (emission measure), the flux ratio is independent on these parameters. Moreover, the exposure time used in the simulations was large enough to ensure negligible statistical errors.

We then modeled the continuum of the simulated spectra with a bremsstrahlung model, fixing the temperature to that used for the simulation, and fitting the normalization using the data in energy intervals of 5 – 6 and 9 – 10.5 keV. We then modeled the data in 6 – 7.5 keV band using the bremsstrahlung model fixed as above and adding two Gaussians for the FeXXV and FeXXVI lines. We used the best fit models to obtain the fluxes of the Gaussians (in photons  $\text{cm}^{-2} \text{s}^{-1}$ ) and consequently determined the theoretical flux ratio of these two emission lines as a function of temperature (see Fig.1). The change in relative abundance of FeXXV and FeXXVI ions with temperature is reflected in the above curves, resulting in a decreasing flux ratio of FeXXV-to-FeXXVI emission lines with increasing temperature, from value of 14 at 4 keV to unity at 11 keV. At low temperatures the model ratio is very sensitive to the variation in temperature (between 4.0 and 4.5 keV the ratio changes from 14 to 10) while it is less sensitive at high temperatures (between 10.5 and 11.0 keV the ratio changes from 1.1 to 1.0).

### 3.2. Results

Next, we measured the line flux ratio in the cluster PN data by fitting the 6.0 – 7.5 keV (5.5 – 7.0 keV) band for Coma (A1795) with an absorbed emission model consisting of bremsstrahlung component and two Gaussians.

We chose to use these narrow bands instead of the full spectra in order to minimize the dependence on calibration accuracy. Indeed, using 2.0 – 7.0 keV band for the fit leads to slightly larger FeXXV-to-FeXXVI ratio, but the corresponding variation in temperature is negligible. Furthermore, using only the narrow band around the iron lines results in a best fit that better describes the line shapes, because of the higher relative importance of the line photons in the  $\chi^2$  sum.

We defined the FeXXV line flux as FeXXVI line flux multiplied by a constant and allowed this constant to vary, together with the FeXXVI normalization, thereby giving the line flux ratio directly. We let also all the bremsstrahlung parameters vary, as well as the gaussian widths and line centroids. In the error analysis, the above parametrization of the line ratio takes properly into account parameter correlations. When searching for the best fit, line centroids were allowed to vary due to possible gain calibration inaccuracies, but the best fit values are virtually the same as predicted. In the error analysis of the spectrum in 2 – 5' region of A1795, the model has too much freedom compared to the quality of the data, resulting in a complicated  $\chi^2$  distribution. Thus, for the line ratio error analysis, we fixed the line energies to the best fit values for all spectra, but this had only effect in the outer part of A1795.

The best fit models are shown in Fig. 2 and the corresponding temperature values are reported in Table 2. At 90% confidence the constraints of the flux ratio for Coma within radii 0–5–13' are  $1.6^{+0.9}_{-0.6}$  and  $2.2^{+0.9}_{-0.6}$  and for A1795 within radii 0–2–5' they are  $5.6^{+2.4}_{-1.7}$  and  $4.2^{+2.7}_{-1.2}$ . The relative uncertainties of the line flux ratio range between 30–70% without no trend as a function of temperature, since the strengths of the two lines behave in opposing ways when varying the temperature. However, as seen above, at lower temperatures the model is much more sensitive to temperature, i.e. at low temperatures a similar variation in line ratio corresponds to smaller variation in tempera-

TABLE 3

Results of single temperature MEKAL fit to 0.3 – 7.0 keV PN data using 0% or 5% systematic errors and various values of  $N_{\text{H}}$ . The statistical errors of  $N_{\text{H}}$  is  $\sim 1 \times 10^{19}$  atoms  $\text{cm}^{-2}$ . The  $\chi^2$  and the 90% confidence interval of  $N_{\text{H}}$  are shown when  $N_{\text{H}}$  is treated as a free parameter

radii	d.o.f.	0%	5%	5%, $N_{\text{H}}$ free	$N_{\text{H}}^a$	$N_{\text{HG}}^b$	$N_{\text{HG}}^c$
		$\frac{\chi^2}{d.o.f.}$	$\frac{\chi^2}{d.o.f.}$	$\frac{\chi^2}{d.o.f.}$			
<b>Coma</b>							
0'– 5'	176	3.46	0.93	0.77	$0^{+0.1}$	0.9	0.9
5'– 13'	176	6.72	1.11	0.90	$0^{+0.1}$	0.9	0.9
<b>A1795</b>							
0'– 2'	177	4.04	1.11	0.94	$0^{+0.2}$	1.0	1.2
2'– 5'	176	2.76	1.04	0.91	$0^{+0.3}$	1.0	1.2
<b>3112</b>							
0'– 1.5'	177	3.32	1.48	1.06	$0.2^{+0.5}_{-0.2}$	2.5	
1.5'– 4.5'	177	1.90	1.28	1.04	$0.7^{+0.5}_{-0.6}$	2.5	

a:  $N_{\text{H}}$  as a free parameter, in  $10^{20}$  atoms  $\text{cm}^{-2}$

b: fine beam 21 cm  $N_{\text{H}}$ , in  $10^{20}$  atoms  $\text{cm}^{-2}$  (Murphy et al. in prep.)

c: broad beam 21 cm  $N_{\text{H}}$ , in  $10^{20}$  atoms  $\text{cm}^{-2}$  (Dickey & Lockman 1990)

ture than at high temperatures. Thus, similar observable constraints in line ratio lead to better constraints in the model temperature in A1795, compared with Coma. At the lowest temperatures (4 keV) the FeXXVI line is weak and in case of A3112 it reaches the level of noise and thus the flux ratio of A3112 is uninformative. The resulting temperature values are discussed further in Section 4.

#### 4. PROBLEMS WITH ISOTHERMAL MODELING

We then modeled the whole 0.3 - 7.0 keV energy band data of PN with a single MEKAL model (Mewe et al, 1995) absorbed by an HI column density ( $N_{\text{H}}$ ) obtained with a fine beam aperture (20', Murphy et al. in prep.), except for A3112, for which only the wide beam (1°) value is available. We modeled the data without systematic errors, resulting in unacceptable fits (see Table 3 and Fig. 3). Between 0.5 and 1.0 keV there is a systematic positive deviation of the data from model at the 5 – 10 % level. Between 1 and 4 keV there are negative residuals at the 10% level and above 4 keV the positive residuals increase monotonically, reaching 20% at 7 keV. Such large excursions are not consistent with the current understanding of the PN calibration (e.g. Briel, 2001; Kirsch, 2002). Thus the 10% and 20% residuals, respectively at 2 – 3 keV and above 5 keV disagree strongly with the reported residuals of a few % at 2 – 7 keV band using bright point sources with power-law spectra. Addition of 5% systematic errors (see e.g. Griffiths et al. 2002; Kirsch 2002; Snowden et al. 2002) to the whole band leads to improvement of the fits, but yet still not to an acceptable level for all regions in the 3 clusters (see Table 3). Thus, at least one of the components involved in the above analysis, i.e. isothermal model,  $N_{\text{H}}$  from radio measurements or the adopted calibration information, must be wrong.

##### 4.1. Galactic absorption

A possible source of the above residuals is application of the incorrect absorption to the isothermal emission model. To test this scenario, we allowed the  $N_{\text{H}}$  to vary as a free parameter and obtained statistically acceptable fits to PN data. However, the resulting  $N_{\text{H}}$  values are consistent with zero and significantly below the HI column densities measured by narrow beam (20') radio observations at 21 cm wavelengths, where the typical uncertainty is  $\sim 1 \times 10^{19}$   $\text{cm}^{-2}$  (Murphy et al. in prep.). This discrepancy could be explained by assuming that towards the central 13' (Coma) and 5' (A1795 and A3112) cluster regions studied in our work, the Galactic  $N_{\text{H}}$  is by 0.5 - 2.0  $\times 10^{20}$  atoms  $\text{cm}^{-2}$  smaller than that within the central 20' region covered by the radio measurements. But such  $N_{\text{H}}$  depletion in Galaxy, at a direction of these clusters, would be a non-physical co-incidence and thus this explanation fails. Moreover, the  $N_{\text{H}}$  values using broad beam ( $\sim 1^\circ$ , Dickey and Lockman 1990) and narrow beam (20', Murphy et al.) 21 cm data for Coma and A1795 are consistent (Table 3). This further indicates that the galactic HI column density is smoothly distributed in the direction of our clusters, and that the application of  $N_{\text{H}}$  as measured in radio, is accurate.

##### 4.2. Calibration issues

###### 4.2.1. 2 – 7 keV band

To study the accuracy of the high energy band calibration, we fitted the 2 – 7 keV energy band data in PN and MOS separately, using MEKAL model and including 5% systematic errors in the fits. The resulting fits are acceptable, and the best-fit values of temperatures and metal abundances (see Table 4) in PN and MOS are in good agreement. This implies that either the hard band EPIC calibration is accurate or that both PN and MOS are miscalibrated in a similar manner.

The hard band temperatures of Coma and A1795 are

TABLE 4

The results of best fits to PN and MOS data to energy bands of 0.3 – 2.0 keV and 2.0 – 7.0 keV with mekal model. In the fits, we 5% systematic errors and Galactic  $N_{\text{H}}$  are used

	0.3 – 2.0 keV		2.0 - 7.0 keV			
	PN T [keV]	MOS T [keV]	PN T [keV]	abund [Solar]	MOS T [keV]	MOS ab [Solar]
	<b>Coma</b>					
0' – 5'	$4.9^{+0.7}_{-0.4}$	$6.9^{+0.8}_{-0.9}$	$9.2^{+0.7}_{-0.6}$	$0.21^{+0.04}_{-0.04}$	$9.9^{+0.6}_{-0.5}$	$0.23^{+0.03}_{-0.03}$
5' – 13'	$4.8^{+0.5}_{-0.4}$	$6.5^{+0.8}_{-0.7}$	$9.2^{+0.6}_{-0.5}$	$0.20^{+0.04}_{-0.03}$	$9.8^{+0.6}_{-0.4}$	$0.24^{+0.03}_{-0.02}$
	<b>A1795</b>					
0' – 2'	$3.4^{+0.2}_{-0.2}$	$4.6^{+0.4}_{-0.3}$	$5.4^{+0.2}_{-0.3}$	$0.39^{+0.04}_{-0.04}$	$5.5^{+0.3}_{-0.2}$	$0.42^{+0.03}_{-0.03}$
2' – 5'	$4.1^{+0.4}_{-0.3}$	$5.5^{+0.5}_{-0.4}$	$6.7^{+0.4}_{-0.4}$	$0.27^{+0.04}_{-0.04}$	$6.9^{+0.4}_{-0.3}$	$0.29^{+0.03}_{-0.03}$
	<b>A3112</b>					
0' – 1.5'	$2.6^{+0.2}_{-0.1}$	$3.5^{+0.3}_{-0.2}$	$4.6^{+0.3}_{-0.2}$	$0.50^{+0.07}_{-0.06}$	$4.9^{+0.3}_{-0.2}$	$0.47^{+0.04}_{-0.04}$
1.5' – 4.5'	$3.0^{+0.3}_{-0.2}$	$3.4^{+0.3}_{-0.2}$	$5.4^{+0.6}_{-0.4}$	$0.28^{+0.07}_{-0.06}$	$5.1^{+0.4}_{-0.4}$	$0.34^{+0.06}_{-0.05}$

consistent with those obtained using the 2 – 10 keV band data from BeppoSAX (deGrandi & Molendi, 2002). This indicates that there is no significant hard band miscalibration in PN and MOS. Furthermore, in A1795, and in the center of Coma, the line ratio analysis (Section 3) yields temperatures consistent with those of the continuum fit and the MEKAL fit to 2 – 7 keV PN and MOS data. These agreements imply that the hard band calibration of PN and MOS is accurate within the level of the statistical uncertainties in our work. In particular there is no evidence for any systematic trend caused by the 2 – 7 keV miscalibration that biases our application of the MEKAL model to the high energy data. In the outer part of Coma, the continuum temperatures are somewhat higher than the line ratio values. The difference in Coma may be due to non-thermal emission as observed at hard X-ray band with BeppoSAX PDS (Fusco-Femiano et al. 1999). Extrapolating the best-fit power-law spectrum of PDS 20 – 100 keV data to PN energies, and adding the expected PN flux from the hot gas has the effect of flattening the 2–7 keV slope, while leaving the line ratio unchanged. For Coma, we will compare the outcome of using either the line ratio temperatures or the MEKAL fit values in Section 5.1.

#### 4.2.2. 0.3 – 2.0 keV band

In order to assess the low energy band calibration accuracy, we repeated the isothermal analysis in the 0.3 – 2.0 keV energy band. In case of purely isothermal emission, the application of accurate absorption model and accurate high energy band calibration information (as justified above), should yield consistent temperatures in both bands for a given cluster and a given region. However, while the resulting fits to low energy band data are statistically acceptable, they are significantly and systematically different from those obtained in the high energy band (see Table 4). The temperatures derived in the low energy band using PN (MOS) are 2 – 4 keV (1 – 3 keV) smaller than those obtained using the high energy band. These conclusions do not change whether or not we include the cooling

flow regions of A1795 and A3112 in the comparison, i.e. the cooling does not explain these discrepancies. The significant underestimation of the low energy effective areas of PN and MOS, and consequent underprediction of the thermal model would lead to the softening of the best-fit spectra at low energies, or, if the model is kept fixed to that derived using the high energy band data, to soft excess. This would also explain why the fitted  $N_{\text{H}}$  values are much smaller than the radio measurements (see Section 4.1).

However, the published XMM-Newton calibration works on power-law sources like BL-LAC objects (e.g. Briel et al. 2002, Ferrando et al. 2002, Haberl et al. 2002) do not report soft excesses or sub-galactic  $N_{\text{H}}$ . Also, analysis of PN data of a large QSO sample (Akylas et al. 2002) with Galactic  $N_{\text{H}}$  yields no soft excess in these objects. Thus it seems likely that a significant miscalibration is not the reason for the soft excess we observe here. Rather, it is implied that the assumption of isothermality is wrong and that the soft excess is real, as we assume in the following.

## 5. SOFT EXCESS

Extrapolating the 2 – 7 keV band thermal models (see 4.2.1) to soft X-ray energies reveals the soft excess (see Figs. 4,5) in Coma, A1795 and A3112. In all cases, both in PN and MOS, the data are above the model at energies below 2 keV. The excess increases towards lower energies, reaching 20% (40%) of the model level at 0.3 keV for Coma and A1795 (A3112). The difference of the soft excess fraction in A3112 is a further indication that the effect is not due to calibration problems.

### 5.1. Thermal modeling

The residuals above the hot thermal model in the 0.3 – 2.0 keV band exhibit differences at 5% level of the model between PN and MOS, consistent with the calibration residuals (e.g. Briel 2001). This, as a fraction of the soft excess flux maybe large enough to prevent accurate parametrization of the soft component. We thus proceed

TABLE 5

Properties of the thermal soft component. Luminosities are obtained in the 0.2 - 2.0 keV band and are in units of  $10^{43}$  erg  $s^{-1}$ , using  $H = 50$  km  $s^{-1}$  Mpc $^{-1}$ .

radii	PN		MOS		PN + MOS		$L_{warm}$	$\frac{L_{warm}}{L_{hot}}$
	T [keV]	ab [solar]	T [keV]	ab [solar]	T [keV]	ab [solar]		
	<b>Coma</b>							
0' - 5'	$0.84^{+0.16}_{-0.10}$	$0.03^{+0.03}_{-0.02}$	$0.94^{+0.14}_{-0.12}$	$0.00^{+0.02}_{-0.02}$	$0.89^{+0.19}_{-0.15}$	$0.02^{+0.05}_{-0.02}$	$1.1^{+0.3}_{-0.2}$	$0.14^{+0.03}_{-0.03}$
5' - 13'	$0.82^{+0.13}_{-0.08}$	$0.03^{+0.03}_{-0.02}$	$0.90^{+0.11}_{-0.10}$	$0.00^{+0.02}_{-0.02}$	$0.86^{+0.15}_{-0.12}$	$0.02^{+0.04}_{-0.02}$	$3.1^{+0.6}_{-0.6}$	$0.15^{+0.03}_{-0.03}$
	<b>A1795</b>							
0' - 2'	$0.96^{+0.13}_{-0.10}$	$0.06^{+0.06}_{-0.03}$	$1.02^{+0.13}_{-0.14}$	$0.02^{+0.04}_{-0.02}$	$0.99^{+0.17}_{-0.12}$	$0.03^{+0.09}_{-0.03}$	$5.8^{+1.6}_{-1.8}$	$0.15^{+0.04}_{-0.05}$
2' - 5'	$0.86^{+0.18}_{-0.11}$	$0.03^{+0.04}_{-0.02}$	$0.88^{+0.17}_{-0.14}$	$0.00^{+0.01}_{-0.01}$	$0.87^{+0.18}_{-0.13}$	$0.06^{+0.01}_{-0.06}$	$3.6^{+1.2}_{-0.8}$	$0.14^{+0.05}_{-0.03}$
	<b>A3112</b>							
0' - 1.5'	$0.81^{+0.12}_{-0.07}$	$0.02^{+0.02}_{-0.02}$	$1.18^{+0.11}_{-0.14}$	$0.08^{+0.07}_{-0.06}$	$1.00^{+0.29}_{-0.26}$	$0.05^{+0.10}_{-0.05}$	$6.3^{+2.7}_{-1.7}$	$0.22^{+0.09}_{-0.06}$
1.5' - 4.5'	$0.85^{+0.12}_{-0.10}$	$0.02^{+0.02}_{-0.02}$	$0.75^{+0.10}_{-0.14}$	$0.00^{+0.02}_{-0.02}$	$0.80^{+0.17}_{-0.16}$	$0.01^{+0.03}_{-0.01}$	$3.4^{+0.9}_{-0.7}$	$0.22^{+0.06}_{-0.05}$

by modeling PN and MOS data separately, keeping the hot component parameters fixed to the values found above, and allowing a second MEKAL emission component to account for the soft excess. By comparing the output obtained from PN and MOS data we can estimate the level of low energy calibration uncertainties.

The resulting fits (Table 5) are statistically acceptable (see Table 6), with reduced  $\chi^2$  values below unity, indicating that the adopted 5% systematic error in the fits is an overestimate of the real calibration residuals. The PN and MOS data give consistent results for the temperature and metal abundance at all cases. Attributing the small offsets in PN and MOS values to systematic errors, rather than random noise, we take the average values of PN and MOS as best values in each radial bin, and include both PN and MOS statistical uncertainty intervals in the final errors of the temperature, metal abundance and the luminosities. Note that the normalization differences between PN and MOS are included in the uncertainties of the luminosities and they dominate over the effect of the statistical uncertainties of the parameters of the very precisely determined hot component, which were thus ignored in the reported luminosity values.

The results (see Fig. 6) indicate that the soft component has similar temperatures of 0.6 - 1.3 keV in different clusters inside  $0.5 h_{50}^{-1}$  Mpc. The metal abundances are low, below 0.15 solar within uncertainties and in most cases consistent with zero. XSPEC simulations indicate that the metal abundance of 0.05 of a typical best-fit model can be recovered to a good accuracy, i.e. strong emission lines can not be altogether removed by the instrumental redistribution of counts. The luminosities of the warm component in 0.2 - 2.0 keV energy band are consistent in different clusters in radial range 0.2 -  $0.5 h_{50}^{-1}$  Mpc. In the central 0.2 Mpc the 0.2 - 2.0 keV luminosities are consistent within the two cooling flow clusters A1795 and A3112, both being six times higher than in Coma. The 0.2 - 2.0 keV luminosities per metric area of the warm component increase by a

factor of  $\sim 10$  between 0.2 - 0.5 and 0 - 0.2 Mpc in A1795 and A3112. Interestingly, the hot component behaves the same way, producing constant warm-to-hot component luminosity ratio in a given cluster in 0.2 - 2.0 keV energy band  $0.5 h_{50}^{-1}$  Mpc, although a variation by a factor of 2 is allowed by the errors.

By holding the temperature of the hot component at the line ratio values, and normalizing the model to that of 2 - 7 keV flux, one obtains slightly smaller temperatures for the soft component of Coma, but nevertheless consistent with the ones presented above. Further, by letting all the parameters of the hot and warm components vary, one does not arrive at significant difference in the properties of the soft component from the ones presented above.

As an independent check for the existence of the soft excess in these clusters, we plotted the ROSAT PSPC data from Bonamente et al. (2002, A3112 not included) together with the best-fit two-component PN models (Fig. 7). Due to cross-calibration uncertainties between PSPC and PN, we allowed a normalization difference for the model to match the PSPC data at 2 keV energies. However, the differences were small, a few %. The agreement between the XMM-Newton instruments and PSPC is very good in Coma and A1795. The conspiracy of similar calibration problems in PN, MOS and PSPC, which incorporate very different technologies, is extremely unlikely. Thus PSPC data confirm not only the existence but also general spectral features of the soft excess.

## 5.2. Non-thermal

Using a power-law model for the soft component leads to systematically poorer fits (see Table 6), but which are statistically acceptable in all cases, except for the center of A3112. Since most of the reduced  $\chi^2$  values for the thermal fits are below unity, this implies an overestimate of the systematic errors. If the calibration were better than the 5% level, and thus smaller systematic error would affect the model, the thermal fits would probably yield reduced  $\chi^2$  values of unity, and the power-law fits would all become

TABLE 6

Comparison of best-fits to PN data using mekal or power-law to model the soft excess

radii	mekal		power-law	
	$\frac{\chi^2}{d.o.f.}$	d.o.f.	$\frac{\chi^2}{d.o.f.}$	d.o.f.
<b>Coma</b>				
0'– 5'	0.50	176	0.76	177
5'– 13'	0.56	176	0.87	177
<b>A1795</b>				
0'– 2'	0.65	177	1.08	178
2'– 5'	0.73	176	0.96	177
<b>A3112</b>				
0'– 1.5'	0.98	177	1.34	178
1.5'– 4.5'	0.87	177	1.13	178

unacceptable. Thus, although for the moment a firm conclusion of the nature of the soft excess is not available, the thermal model is preferred.

#### 6. SOFT COMPONENT INTERPRETATION

We use the PN and MOS averaged best-fit thermal models obtained above to derive physical properties of the warm and hot components (see Table 7). For the estimate of the electron density, we assume that the observed emission measure originates from a spherical shell of constant density with radii equal to those of the annuli for which the spectra were extracted. The resulting densities of the warm component are similar in different clusters at the same radii ( $2\text{-}4 \times 10^{-3}$  atoms  $\text{cm}^{-3}$  at  $0\text{-}0.2 h_{50}^{-1}$  Mpc and  $0.6\text{-}0.7 \times 10^{-3}$  atoms  $\text{cm}^{-3}$  at  $0.2\text{-}0.5 h_{50}^{-1}$  Mpc), corresponding to overdensities of 1000 - 200 (in terms of the critical density).

The cooling time scale can be estimated using bremsstrahlung cooling function since the line emission is negligible due to the apparent low abundances. Using

$$t_{cool} = 6 \times 10^9 \left(\frac{T}{10^6 \text{K}}\right)^{\frac{1}{2}} \left(\frac{n}{10^{-3} \text{cm}^{-3}}\right)^{-1} \text{years} \quad (1)$$

we obtain cooling times larger or comparable to the Hubble time. The pressure of the ideal (warm) gas,  $\sim 10^{-12}$  erg  $\text{cm}^{-3}$  is an order of magnitude smaller than that of the hot gas.

#### 7. CONCLUSIONS AND DISCUSSION

In galaxy clusters Coma, A1795 and A3112, the hot intracluster gas as determined by modeling the 2 - 7 keV PN and MOS data is consistent with that inferred from the FeXXV-FeXXVI line ratio. This lends confidence to our method of characterizing the hot component by using the 2 - 7 keV band. The expected emission spectrum from

TABLE 7

Physical properties of the thermal components.  $n$  is the atom density,  $\delta$  is the gas density in terms of the critical density.  $P$  gives the gas pressure while  $t_{cool}$  gives the bremsstrahlung cooling time

radii	WARM				HOT			
	$n^a$	$\delta$	$t_{cool}$ ( $10^9$ y)	$P^b$	$n^a$	$\delta$	$t_{cool}$ ( $10^9$ y)	$P^b$
<b>Coma</b>								
0'– 5'	1.5	510	13	2.2	3.5	1180	18	55
5'– 13'	0.6	210	30	0.9	1.4	460	46	21
<b>A1795</b>								
0'– 2'	3.2	970	6	5.2	7.4	2200	6	65
2'– 5'	0.7	200	27	1.0	1.6	460	34	17
<b>A3112</b>								
0'– 1.5'	3.3	940	6	5.6	6.2	1760	7	48
1.5'– 4.5'	0.7	190	27	0.9	1.2	330	40	9.6

a: [ $10^{-3} \text{cm}^{-3}$ ]

b: [ $10^{-12} \text{erg cm}^{-3}$ ]

this component at lower energies may then be computed and compared with the data, during which a significant warm emission component at a level above the systematic uncertainties becomes evident. The non-thermal origin of the phenomenon cannot be ruled out at the current level of calibration accuracy, but the thermal model fits the data better. The warm gas is found to have temperatures of 0.6 – 1.3 keV inside 0.5  $h_{50}^{-1}$  Mpc, consistent with the 90% distribution of the temperature values in Warm Hot Inter-galactic Medium WHIM simulations (Dave et al., 2001). Within 0.2 and 0.5  $h_{50}^{-1}$  Mpc, the derived electron densities ( $\sim 10^{-4} \text{ cm}^{-3}$ ) are marginally consistent with the simulations, but in the cluster cores the derived densities are too high compared to those given by the simulations. This indicates that while WHIM may be a viable explanation for the soft excess at the outer regions of the clusters, it cannot explain the soft excess phenomenon entirely.

While the luminosities of the hot component in Coma, A1795 and A3112 vary substantially, those of the warm component outside the cool core region are consistent in the three clusters being considered. The similarities suggest a common origin for the warm component, independent of the hot gas and its cooling. The derived values for the pressure of the hot component along the central 0.5 Mpc line of sight towards Coma, A1795 and A3112 are an order of magnitude higher than those of the warm gas, suggesting that they are not in contact. These requirements can be satisfied in a WHIM scenario where filaments do not penetrate the clusters, but rather form an external network. In this scenario, the density of the hot gas in clusters drops faster with radius than that of the WHIM filaments. Indeed, in Bonamente et al. (2002) the ROSAT PSPC data pointed to a radial increase of the soft excess.

Thus, at  $\sim 1 h_{50}^{-1}$  Mpc the pressure equipartition may be attained and stable structures like filaments may be maintained. Outside the center, the homogenous distribution of filaments, projected in the cluster direction, produces constant luminosity per  $\text{Mpc}^2$  in different clusters.

One could argue that the central warm component is a result of a cooling flow. However, we note that the central brightness peak is not softening; rather the warm and hot component luminosities are enhanced by a similar factor compared to the outer parts - this is different from the standard cooling flow model where the spectral peak shifts sharply towards low energies in the center. Also, the cooling flow model does not explain the existence of the warm gas outside the cooling radii, as noted in this work. Likewise, the existence of warm gas at the center of Coma cannot be explained by cooling, since the temperature of the hot gas is the same inside and outside the core region of Coma. On the other hand, we already mentioned that in the center of A1795 and A3112 the hot gas cools and the luminosities of the warm and hot gas are enhanced - such phenomena are absent in Coma. This suggests (in the context of the filament model described above) that 1) the central line of sight intersects similar amount of WHIM gas in projected filaments, giving a basic level of radiation ( $\sim 1 \times 10^{44} \text{ erg s}^{-1} \text{ Mpc}^{-2}$ ) common to all clusters; 2) emissions resulting from any cooling of the central hot gas are reprocessed by the overlying layers of warm gas.

J. Nevalainen acknowledges an ESA Research Fellowship, and a NASA grant NAG5-9945. M. Bonamente gratefully acknowledges NASA for support. We thank the referee and Drs. J. Kaastra, M. Markevitch and O. Vilhu for useful comments.

## REFERENCES

- Arabadjis, J.S. and Bregman, J.N. 1999, ApJ, 514,607  
 Arnaud, M., Aghanim, N., Gastaud, R. et al. 2001a, A&A 365, L67  
 Arnaud, M., Neumann, D., Aghanim, N. et al., 2001b, A&A 365, L80  
 Akylas, A., Georgantopoulos, I. & Barcons, X., 2002, submitted to A&A, astro-ph/0205549  
 Berghoefer, T.W. and Bowyer, S. 2002, ApJ, 565, L17  
 Briel 2002, in Proceedings of the Symposium ‘New Visions of the X-ray Universe in the XMM-Newton and Chandra era’, 26-30 November 2001, ESTEC, Noordwijk, The Netherlands  
 Bonamente, M., Lieu, R., Joy, M. & Nevalainen, J., 2002, ApJ, 576, 688  
 Bonamente, M., Lieu, R. & Mittaz, J., 2001a, ApJ, 547,7  
 Bonamente, M., Lieu, R. & Mittaz, J., 2001b, ApJL, 561, 63  
 Bonamente, M., Lieu, R., Nevalainen, J & Kaastra, J., 2001c, ApJL, 552, 7  
 Bonamente, M., Lieu, R. & Mittaz, J., 2001d, ApJ, 546, 805  
 Bowyer, S., Berghoefer, T.W. and Korpela, E.J. 1999, ApJ, 526, 592  
 Buote, D., 2001, ApJ, 548, 652  
 Cen, R. & Ostriker, J., 1999, ApJ, 514, 1  
 Cen, R., Tripp, T., Ostriker, J. & Jenkins, E., 2001, ApJL, 559, 5  
 Davé, R., Cen, R., Ostriker, J. et al., 2001, ApJ, 552, 473  
 De Grandi S., & Molendi, S., 2002, ApJ, 567, 163  
 Dickey, J. & Lockman, F., 1990, ARAA, 28, 215  
 Ferrando, P., Abbey, F., Altieri, B. et al. 2002, Proceedings of the Symposium ‘New Visions of the X-ray Universe in the XMM-Newton and Chandra era’, 26-30 November 2001, ESTEC, Noordwijk, The Netherlands, astro-ph/0202372  
 Fusco-Femiano, R., dal Fiume, D., Feretti, L. et al., 1999, ApJL, 513, 21  
 Griffiths, G., Briel, U., Dadina, M., et al., 2002, Proceedings of the Symposium ‘New Visions of the X-ray Universe in the XMM-Newton and Chandra era’, 26-30 November 2001, ESTEC, Noordwijk, The Netherlands  
 Haberl, F., Bennie, P., Briel, U. et al. 2002, Proceedings of the Symposium ‘New Visions of the X-ray Universe in the XMM-Newton and Chandra era’, 26-30 November 2001, ESTEC, Noordwijk, The Netherlands  
 Hwang, 1997, Sci 278, 1917  
 Kaastra, J., Lieu, R., Bleeker, J., Mewe, R. and Colafrancesco, S. 2002, ApJ, 574, L1  
 Kaastra, J., Lieu, R., Mittaz, J., Bleeker, J., Mewe, R., Colafrancesco, S. and Lockman, F. 1999, ApJ, 519, L119  
 Kirsch 2002, Proceedings of the Symposium ‘New Visions of the X-ray Universe in the XMM-Newton and Chandra era’, 26-30 November 2001, ESTEC, Noordwijk, The Netherlands  
 Lieu, R., Bonamente, M. and Mittaz, J.P.D. 1999a, ApJ, 517, L91  
 Lieu, R., Bonamente, M., Mittaz, J.P.D., Durret, F., Dos Santos, S. and Kaastra, J. 1999b, ApJ, 527, L77  
 Lieu, R., Mittaz, J.P.D., Bowyer, S., Lockman, F.J., Hwang, C. -Y., Schmitt, J.H.M.M. 1996a, ApJ, 458, L5  
 Lieu, R., Mittaz, J.P.D., Bowyer, S., Breen, J.O., Lockman, F.J., Murphy, E.M. & Hwang, C. -Y. 1996b, Science, 274, 1335  
 Lieu, R., Axford, W. & Bonamente, M., 1999, ApJL, 510, 25  
 Lumb, D., Warwick, R., Page, M., De Luca, A., 2002, A&A, 389, 93L  
 Marty, P., Kneib, J, Sadat, R., et al., SPIE vol.4851 in press, astro-ph/0209270  
 Mittaz, J.P.D., Lieu, R. and Lockman, F.J. 1998, ApJ, 498, L17  
 Mewe R., Kaastra J. & Liedahl D., 1995, ‘Update on meka: mekal’, Legacy 6, 16  
 Sarazin, C. & Lieu, R., 1998, ApJL, 494, 177  
 Snowden, S., 2002, Proceedings of the Symposium ‘New Visions of the X-ray Universe in the XMM-Newton and Chandra era’, 26-30 November 2001, ESTEC, Noordwijk, The Netherlands, astro-ph/0203311  
 Tamura, T., Kaastra, J., Peterson, J. et al., 2001, A&A 365, L87

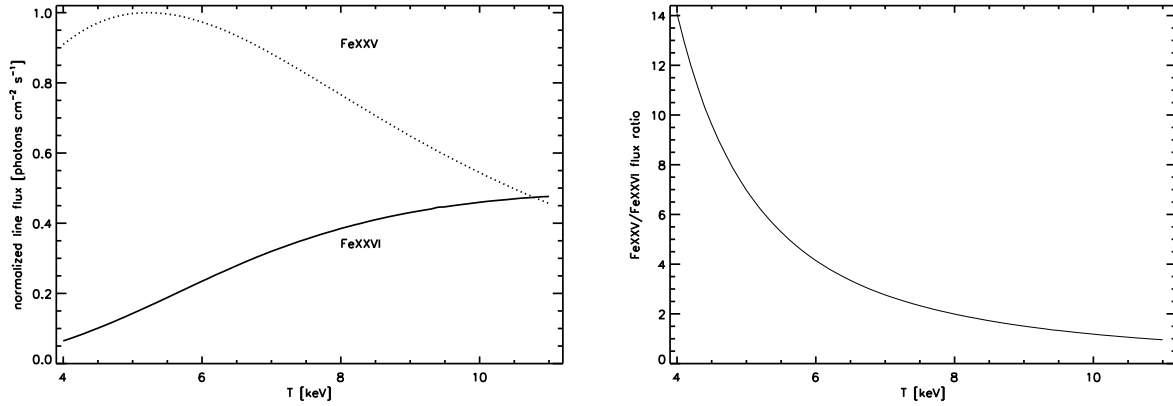


FIG. 1.— The fluxes of FeXXV and FeXXVI emission lines in the mekal model (scaled to the maximum flux of FeXXV) (left panel) and their ratio (right panel) as a function of the electron temperature .

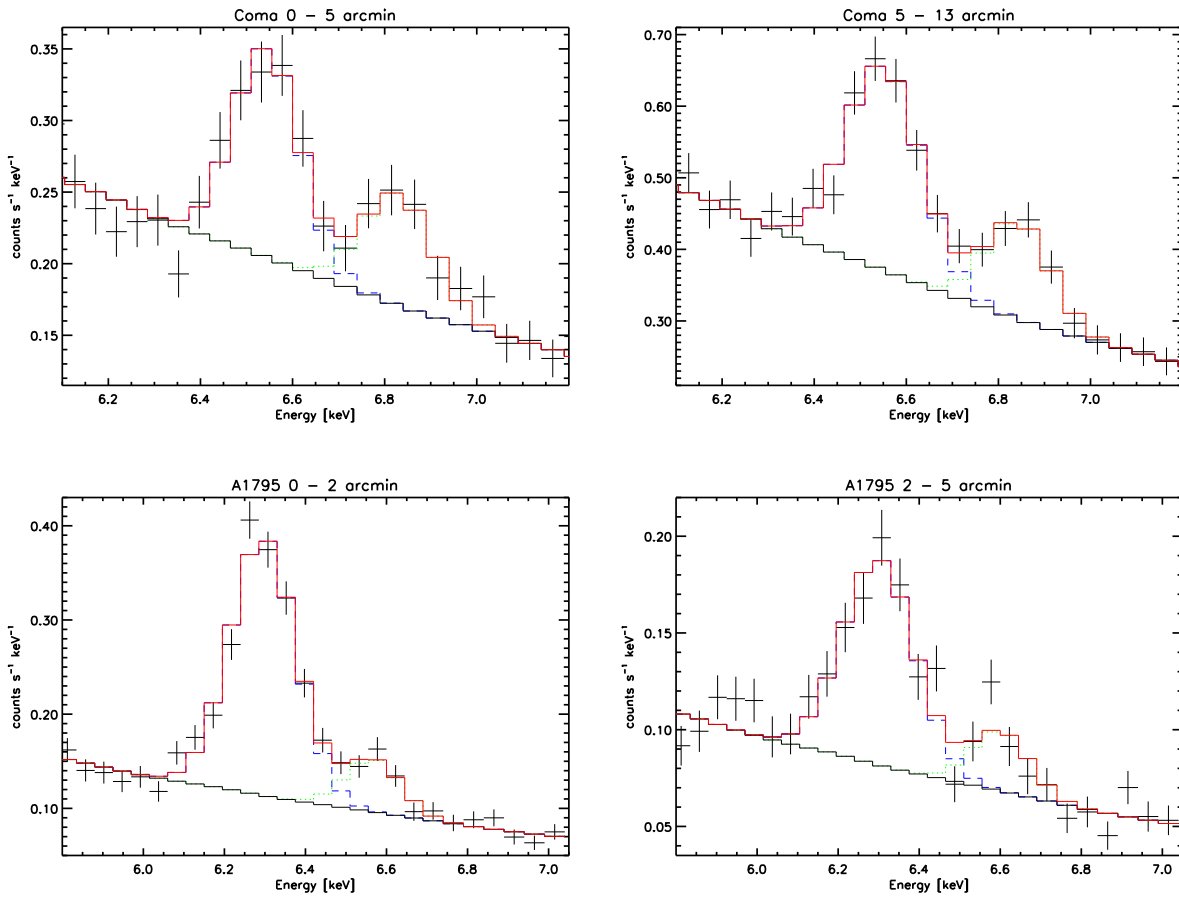


FIG. 2.— The PN spectra of Coma and A1795 around the FeXXV and FeXXVI lines with  $1\sigma$  uncertainties shown as crosses. The folded models for the continuum with and without the Gaussians added are shown as solid lines. The dashed (blue) and the dotted (green) lines show the FeXXV and FeXXVI lines separately.

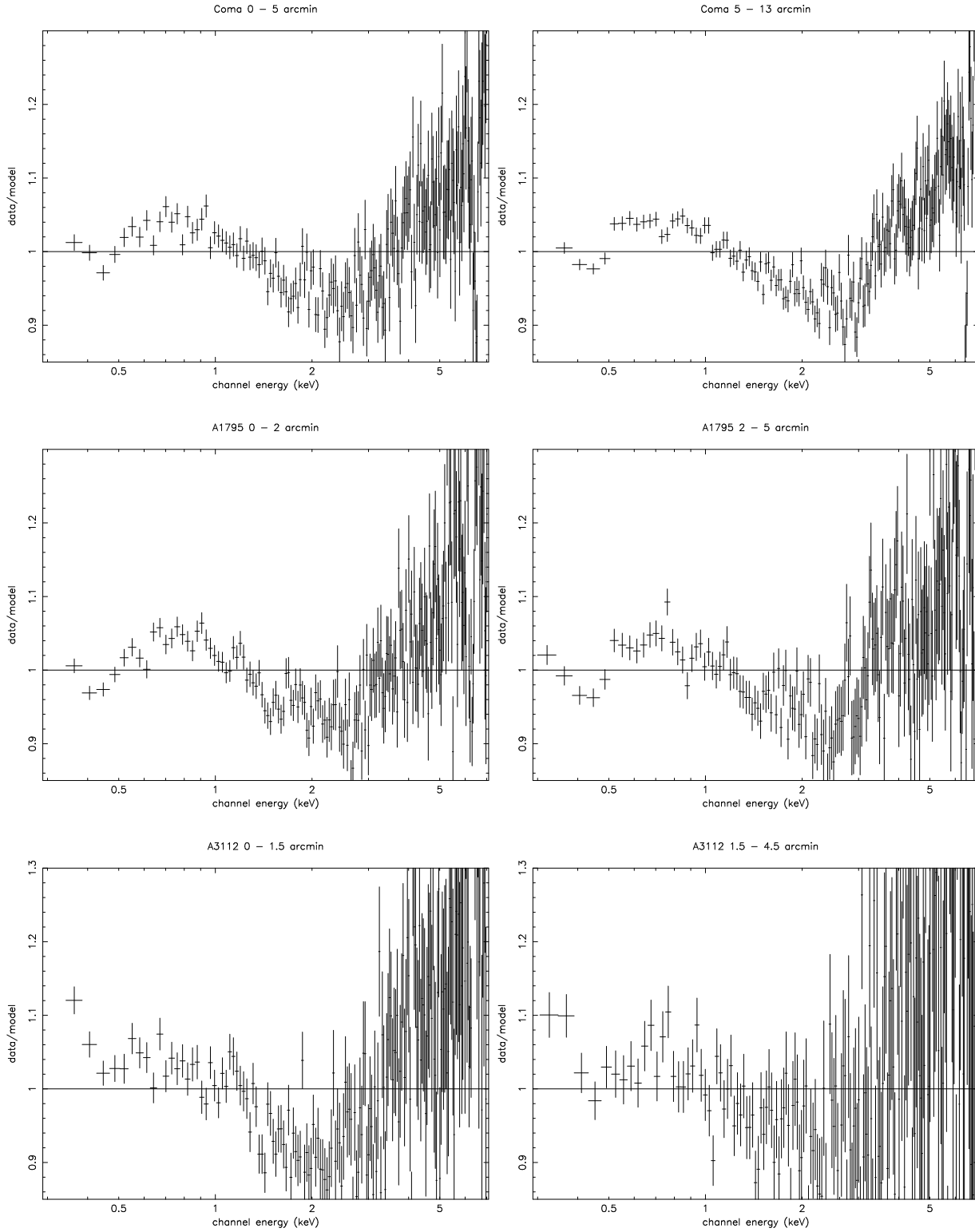


FIG. 3.— The ratio of the PN data of Coma, A1795 and A3112 to the best fit single temperature model to the 0.3 - 7.0 keV band. When modeling the data no systematic errors were added.

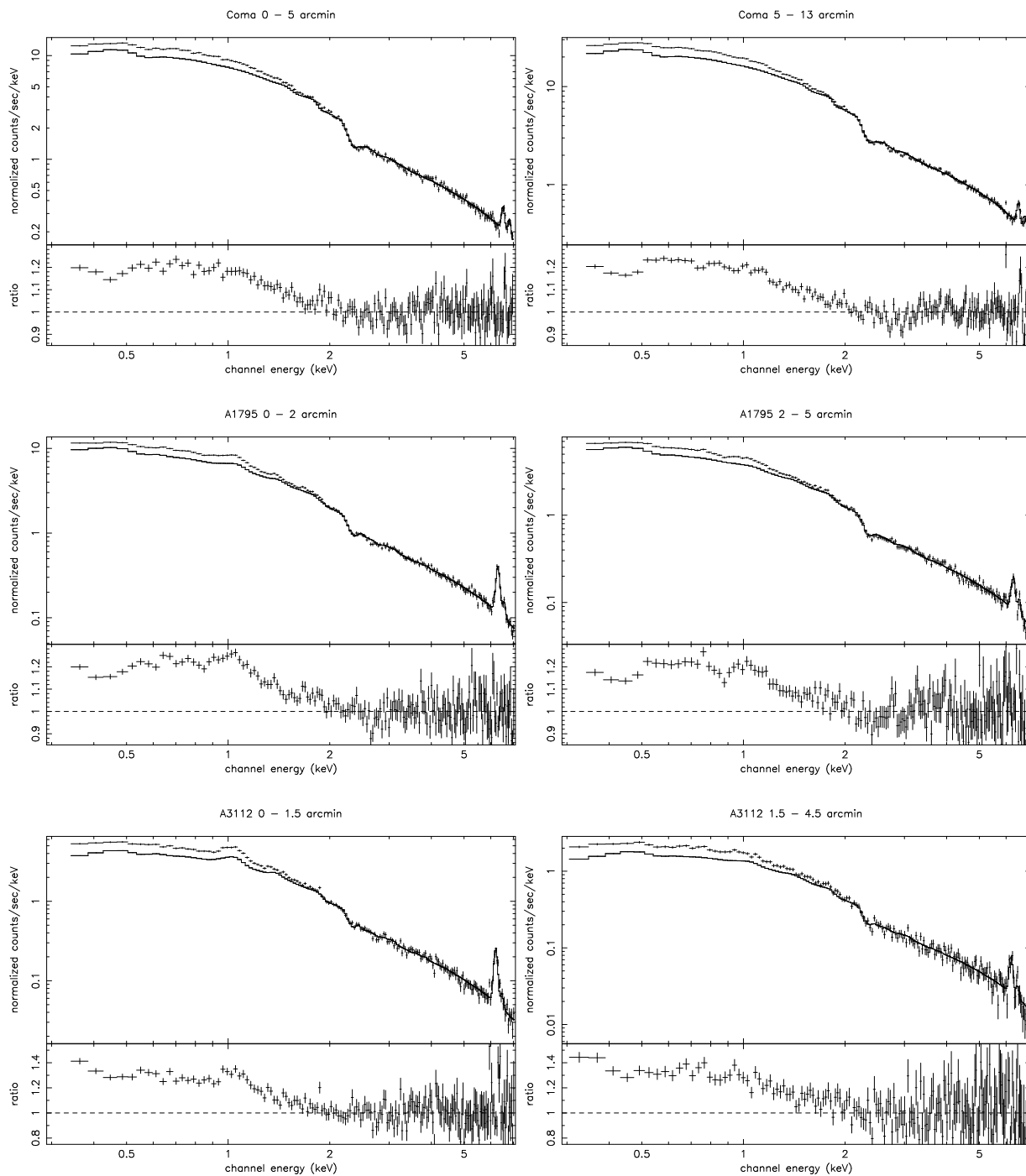


FIG. 4.— The PN data of Coma, A1795 and A3112 with  $1\sigma$  statistical uncertainties. The solid line shows the best fit single temperature fit to 2 – 7 keV data. Lower panels show the ratio of the data to the extrapolated model.

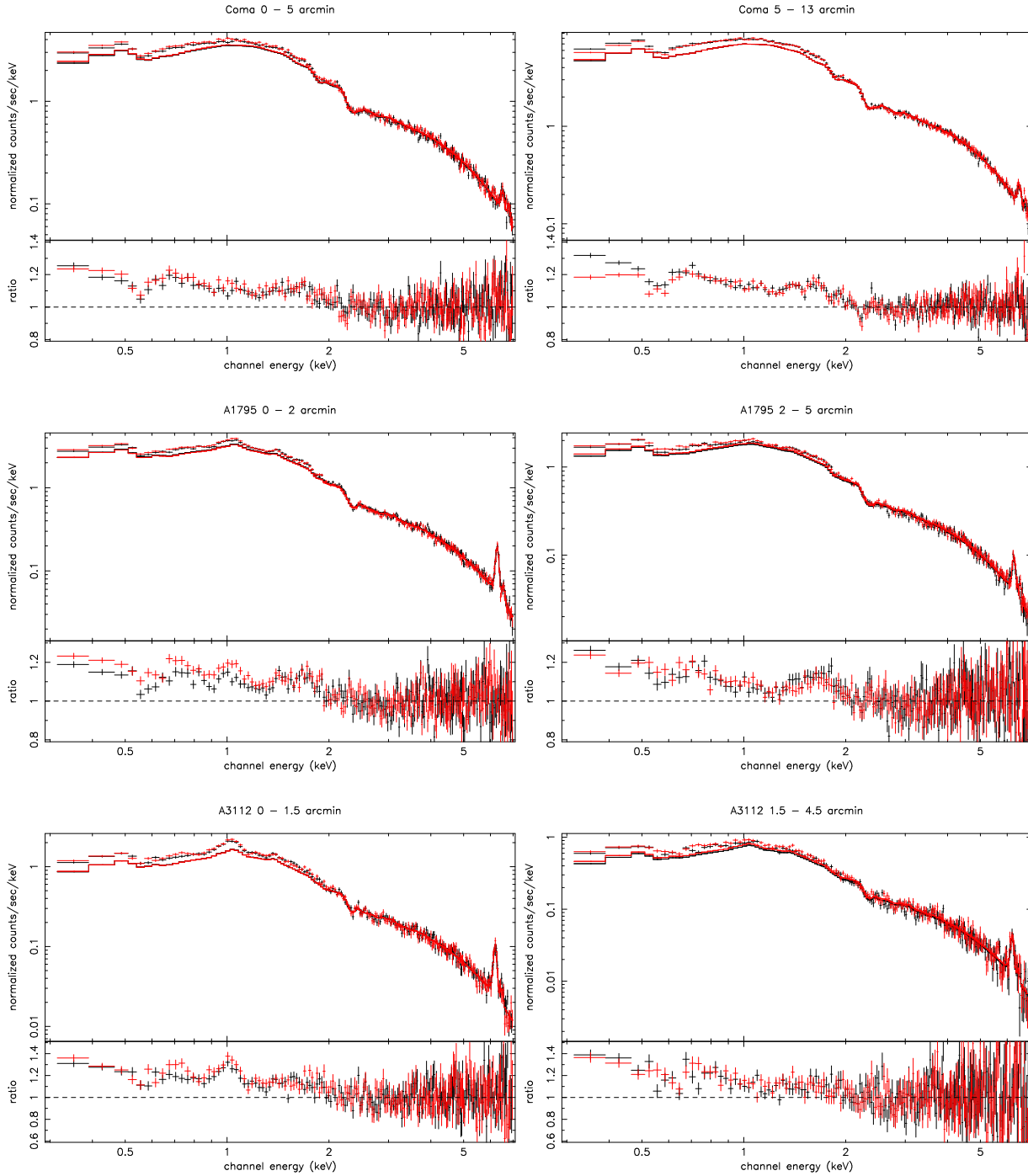


FIG. 5.— Same as Fig. 4, but for MOS.

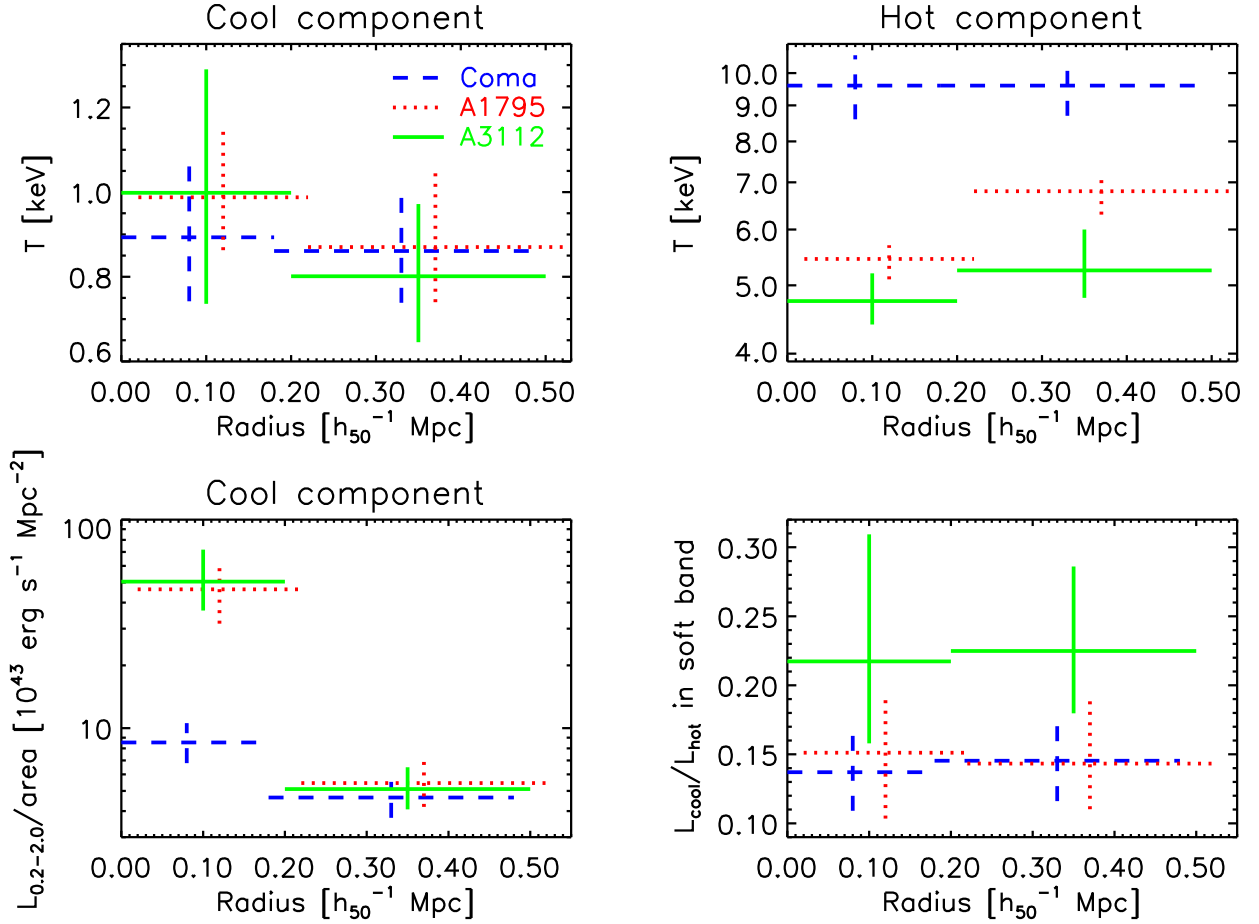


FIG. 6.— The best-fit values and 90% confidence uncertainties for the warm component using a thermal model (left panels). Upper right panel shows the temperatures of the hot component. Blue (dashed), red (dotted) and green (solid) lines correspond to Coma, A1795 and A3113, respectively. The radial bin values (0–0.2–0.5 Mpc) have been shifted slightly for display purposes. Lower right panel shows the ratio of the luminosities of the hot and warm component in 0.2 – 2.0 keV band.

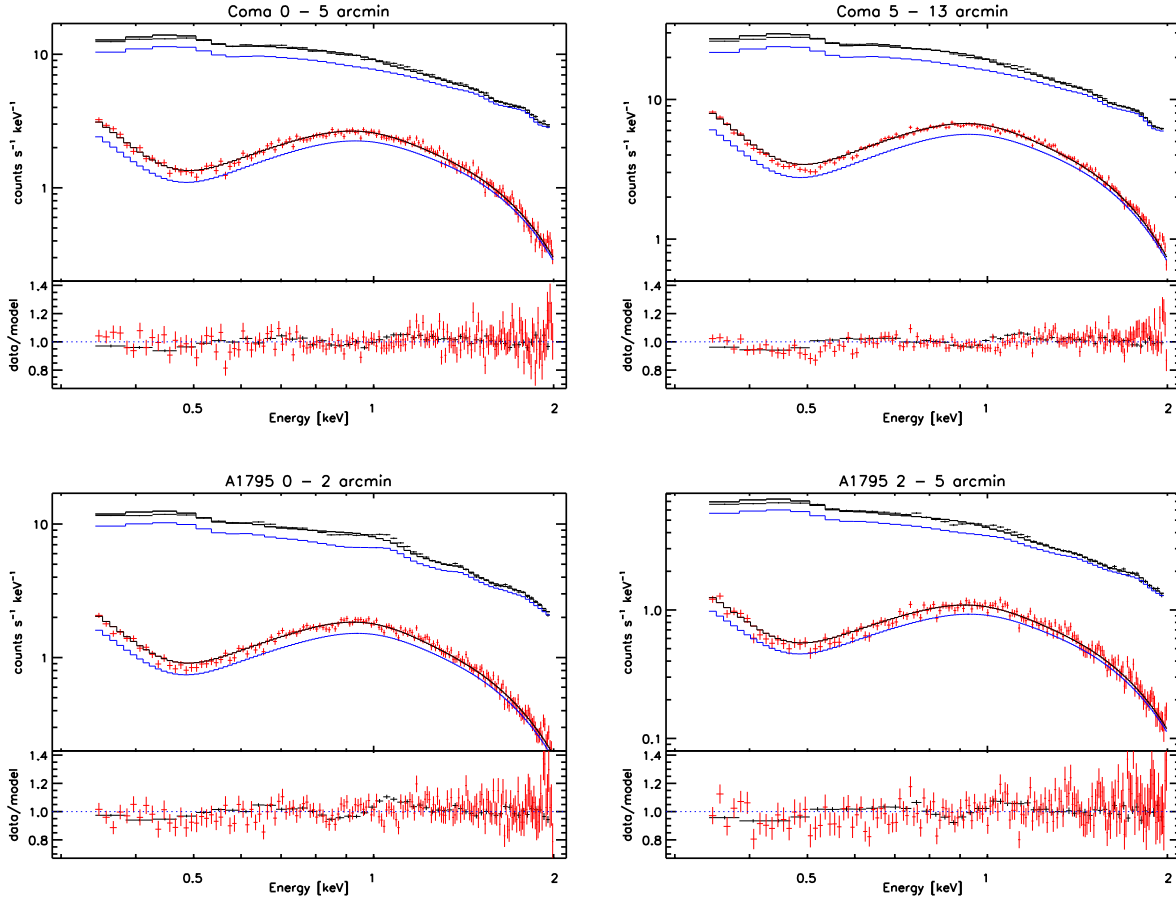


FIG. 7.— The solid black lines show the best fit PN two-component models convolved with the PN and PSPC responses. The solid blue lines show the hot gas component separately. The PN data and the published ROSAT PSPC data (Bonamente et al. 2002) are shown as black and red crosses, respectively. The lower panel shows the data-to-model ratio. The error bars show the  $1\sigma$  statistical uncertainties.